OPTICA

Quantum-limited optical lever measurement of a torsion oscillator

C. M. Pluchar, A. R. Agrawal, and D. J. Wilson*

Wyant College of Optical Sciences, University of Arizona, Tucson, Arizona 85721, USA
**dalziel@optics.arizona.edu*

Received 22 November 2024; revised 25 February 2025; accepted 25 February 2025; published 14 March 2025

The optical lever is a precision displacement sensor with broad applications. In principle, it can track the motion of a mechanical oscillator with added noise at the standard quantum limit (SQL); however, demonstrating this performance requires an oscillator with exceptionally high torque sensitivity or, equivalently, zero-point angular displacement spectral density. Here, we describe optical lever measurements on Si_3N_4 nanoribbons possessing $Q > 3 \times 10^7$ torsion modes with torque sensitivities of 10^{-20} Nm/$\sqrt{\text{Hz}}$ and zero-point displacement spectral densities of 10^{-10} rad/$\sqrt{\text{Hz}}$. By compensating for aberrations and leveraging immunity to classical intensity noise, we realize angular displacement measurements with imprecisions 20 dB below the SQL and demonstrate feedback cooling, using a position-modulated laser beam as a torque actuator, from room temperature to ∼5000 phonons. Our study signals the potential for a new class of torsional quantum optomechanics.

https://doi.org/10.1364/OPTICA.549814

Optical metrology enables precise tracking of mechanical oscillators. This is a key paradigm in the search for new physics, as mechanical oscillators can transduce weak forces such as radiation pressure [1], gravitational waves [2], and electrostatic force [3] into tangible displacements. In the last decade, optomechanical measurements have reached a regime where their added noise is limited by quantum fluctuations of the light field, including radiation pressure shot noise [4]. Subsequently, squeezed light [5] and backaction-evading [6,7] techniques have provided reductions in quantum noise, leading to force and displacement measurements below the standard quantum limit (SQL) [8,9]. This has allowed for a new generation of fundamental physics experiments with even greater sensitivity, which may be useful for dark matter searches [10] and novel tests of gravity [11].

While theory and experiment in optical displacement measurement have focused on interferometry, the quantum limits of alternative techniques, such as the optical lever (OL), have been largely ignored. The OL is notable because of its long history as a precision measurement tool [12], including direct measurements of radiation pressure [1] and gravity [13,14], and its employment in commercial atomic force microscopes [15]. Moreover, there is no fundamental advantage to interferometry, as previous analyses indicate that the displacement sensitivity of the OL is on par [16,17]. While the quantum limit of the OL and the closely related lateral beam displacement problem have been studied [18–21], including enhancement using squeezed light [19,22,23], radiation pressure quantum backaction was not accounted for. As contributions of both imprecision and backaction enforce the SQL, this remains an unexplored regime. A notable exception is the recent demonstration of classical backaction evasion in an OL [24], which has heavily influenced our study.

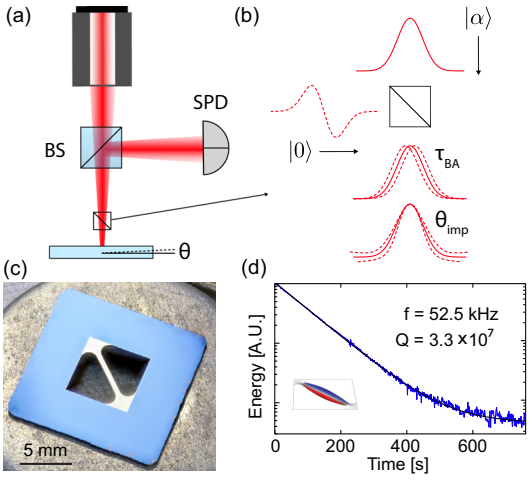

Fig. 1. (a) Sketch of an optical lever measuring angular displacement θ using a split photodetector (SPD). (b) Quantum noise model: the incident field in a HG_{00} coherent state beats against the HG_{10} vacuum, resulting in uncertainty in the incidence angle θ (imprecision) and position x (backaction) due to phase and amplitude vacuum noise, respectively. (c) Photo of a 400 μm wide Si_3N_4 nanoribbon [26]. (d) Ringdown of the nanoribbon's fundamental torsion mode (inset).

In this paper, we present a platform to explore the quantum limits of the OL and angular displacement measurements. Two challenges need to be addressed: first, the thermal torque noise of the mechanical oscillator S_τ^{th} (here expressed as a single-sided

power spectral density evaluated at resonance) needs to be made comparable to the quantum backaction torque S_τ^{BA}. Second, the optical receiver must possess a high quantum efficiency η, in the sense that the product of the backaction and measurement imprecision S_θ^{imp} approaches the Heisenberg limit $S_\theta^{\mathrm{imp}} S_\tau^{\mathrm{BA}} = \hbar^2/\eta \geq \hbar^2$ or equivalently, the total measurement noise approaches the SQL, $S_\theta^{\mathrm{imp}} + S_\theta^{\mathrm{BA}} \geq S_\theta^{\mathrm{ZP}}$, where S_θ^{ZP} is the oscillator's zero-point motion [25].

To address these challenges, we probe Si_3N_4 nanoribbons [26] possessing $Q > 3 \times 10^7$ torsion modes with thermal torques of $S_\tau^{\mathrm{th}} \sim (10^{-20}\,\mathrm{Nm}/\sqrt{\mathrm{Hz}})^2$ and zero-point spectral densities of $S_\theta^{\mathrm{ZP}} \sim (10^{-10}\,\mathrm{rad}/\sqrt{\mathrm{Hz}})^2$. For the receiver, we use a split photodetector, which is known to produce a near-ideal $\eta = 2/\pi$ OL measurement [20,27]. We also carefully account for aberrations stemming from the finite size and curvature of the nanoribbon and exploit access to large optical powers afforded by the relative immunity of the OL to classical intensity noise.

A sketch of the experiment is shown in Fig. 1(a). Light from a laser (wavelength λ) in the fundamental Hermite–Gaussian (HG_{00}) mode is focused onto the ribbon to a spot size ($1/e^2$ intensity radius) w_0, corresponding to the diffraction angle $\theta_{\mathrm{D}} = \lambda/(\pi w_0)$. In the small displacement limit $\theta \ll \theta_{\mathrm{D}}$, the field reflected from the ribbon can be written as a superposition of HG_{00} and HG_{10} modes [24,28]:

$$E_{\mathrm{r}} \approx A_{00} u_{00} + (A_{10}^{\theta} + A_{10}^{\mathrm{vac}}) u_{10}, \tag{1}$$

where u_{00} (u_{10}) is the HG_{00} (HG_{10}) mode shape, and $A_{10}^{\theta} = 2i\theta/\theta_{\mathrm{D}}$ is the amplitude of the HG_{10} mode.

A split photodetector (SPD) placed in the far field of the ribbon acts as a HG_{10} mode sorter, producing a photocurrent proportional to A_{10}^{θ} and, therefore, θ. In Eq. (1), we have included a term A_{10}^{vac} representing vacuum fluctuations of the HG_{10} mode. As illustrated in Fig. 1(b), these fluctuations produce angular and lateral beam displacement noise, yielding imprecision S_θ^{imp} and backaction S_τ^{BA}, respectively. Referring to an apparent angular displacement, the total SPD output can be written as

$$S_\theta[\omega] = S_\theta^{\mathrm{imp}} + |\chi[\omega]|^2 \left(S_\tau^{\mathrm{BA}} + S_\tau^{\mathrm{th}} + 2\hbar |\chi^{-1}[\omega_{\mathrm{m}}]| \right), \tag{2a}$$

$$= S_\theta^{\mathrm{imp}} + S_\theta^{\mathrm{BA}}[\omega] + S_\theta^{\mathrm{th}}[\omega] + S_\theta^{\mathrm{ZP}}[\omega], \tag{2b}$$

where $\chi[\omega] = I^{-1}/(\omega^2 - \omega_{\mathrm{m}}^2 - i\gamma_{\mathrm{m}}\omega)$, ω_{m}, γ_{m}, and I are the mechanical susceptibility, frequency, damping rate, and moment of inertia of the torsion mode, respectively; $S_\tau^{\mathrm{th}} \approx 4k_{\mathrm{B}} T I \gamma_{\mathrm{m}}$ is the thermal torque in the high-temperature limit ($T \gg \hbar\omega_{\mathrm{m}}/k_B$); and S_θ^{BA} and S_θ^{th} are the backaction and thermal displacement, respectively.

As shown in Refs. [24,26,29] and in Supplement 1, placing the SPD in the far field yields an imprecision:

$$S_\theta^{\mathrm{imp}} \approx \frac{\theta_{\mathrm{D}}^2}{8N} \frac{\pi}{2\eta_{\mathrm{d}}} = \frac{1}{w_0^2} \frac{\hbar c \lambda}{4\pi P} \frac{\pi}{2\eta_{\mathrm{d}}}, \tag{3}$$

where $N(P)$ is the photon flux (optical power) on the photodetector, and η_{d} is its quantum efficiency.

Likewise, the radiation pressure backaction torque on the ribbon can be expressed as [24,29] (see Supplement 1)

$$S_\tau^{\mathrm{BA}} = \frac{8N}{\theta_{\mathrm{D}}^2} \frac{w^2}{w_0^2} \hbar^2 = w^2 \frac{4\pi\hbar P}{c\lambda}, \tag{4}$$

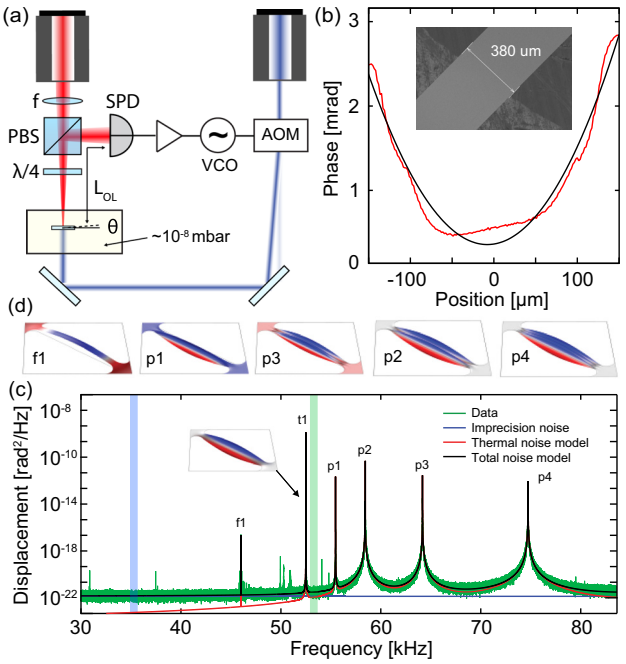

Fig. 2. (a) Experimental setup. The nanoribbon is housed in a vacuum chamber at 10^{-8} mbar. An auxiliary acousto-optic modulated (AOM) beam is used for radiation pressure backaction simulation and feedback control. (b) White light profile of the ribbon near its midpoint, exhibiting effective parabolic curvature. (c) Typical displacement signal showing the torsion mode of interest (t1), "potato chip" modes (p1, p2, p3, p4), and a weakly coupled flexural mode (f1). The total noise model includes thermal noise and imprecision noise. (d) Finite element simulations of the various ribbon modes.

where w is the spot size on the ribbon.

Combining Eqs. (3) and (4), the imprecision–backaction product for the optical lever can be written as

$$S_\theta^{\mathrm{imp}} S_\tau^{\mathrm{BA}} = \frac{\hbar^2}{\eta_{\mathrm{SD}} \eta_{\mathrm{d}}} \frac{w^2}{w_0^2}, \tag{5}$$

where $\eta_{\mathrm{SD}} = 2/\pi$ characterizes the intrinsic nonideality of the SPD, stemming from its inability to distinguish HG_{00} and HG_{10} modes [18,20,27]. The final term w^2/w_0^2 corresponds to excess backaction if the spot size on the ribbon is larger than the beam waist, implying that focusing on the ribbon ($w = w_0$) gives the optimal imprecision [16] and imprecision–backaction product.

Details of the experiment are shown in Fig. 2(a). For the OL, we use $\lambda = 850$ nm light from a Ti-Sapphire laser (red). The light is passed through an optical fiber followed by a collimating lens (not shown) to produce a near-diffraction-limited HG_{00} beam. A second lens (f) focuses the beam on the ribbon, and the return beam is directed to a SPD via a polarizing beamsplitter (PBS). The beam waist w_0, focal position relative to the sample z, and detector-sample separation (optical lever arm) L_{OL} are important parameters for optimizing sensitivity. Nominally, we arrange the setup so that $2w_0 < w_{\mathrm{r}}$, $z \lesssim z_0$, and $L_{\mathrm{OL}} = 0.49\,\mathrm{m} \gg z_0$, where w_{r} is the sample (ribbon) width and $z_0 = \pi w_0^2/\lambda$ is the beam's Rayleigh length.

In addition to the OL, we introduce an auxiliary position-modulated 633 nm laser as a radiation pressure torque actuator. Following Ref. [24], position modulation is achieved by passing

the beam through a frequency-modulated acousto-optic modulator. A dichroic filter (not shown) is used to isolate the SPD from this laser.

Our mechanical oscillator is a Si_3N_4 nanoribbon with length $L \approx 7$ mm, width $w_r = 400$ μm, thickness $h = 75$ nm [Fig. 1(c)], fundamental torsion mode frequency $\omega_m = 2\pi \times 52.5$ kHz $\approx (\pi/L)\sqrt{\sigma/\rho}$, and finite-element-simulated moment of inertia $I = 3.8 \times 10^{-18}$ kg m$^2 \approx \rho L h w_r^3/24$, where $\sigma \approx 0.85$ GHz and $\rho \approx 2700$ kg/m^3 are the ribbon tensile stress and density, respectively. Previously [26], we found that strain-induced dissipation dilution in these ribbons yields torsional Q factors as high as $Q_0 \sigma w_r^2/(E h^2) \approx 10^8$, where E and Q_0 are the ribbon elastic modulus and intrinsic Q. This is attractive because it implies access to exceptionally high torque sensitivities and zero-point spectral densities through the scaling laws $S_\tau^{th} = 4k_B T I \omega_m/Q \propto h^3 w_r/Q_0$ and $S_\theta^{ZP} = 2\hbar Q/(I\omega_m^2) \propto Q_0/(h^3 w_r L)$ [26] (motivating the use of wider, thinner devices). Specifically, for the device used in this study, we measure $Q = 3.3 \times 10^7$ via ringdown [Fig. 2(c)], corresponding to $S_\theta^{th} \approx (2.5 \times 10^{-20}$ Nm/$\sqrt{\text{Hz}})^2$ and $S_\theta^{ZP} = (1.3 \times 10^{-10}$ rad/$\sqrt{\text{Hz}})^2$.

Figure 3 shows a set of experiments aimed at optimizing the efficiency of an OL measurement performed on the fundamental torsion mode of a nanoribbon. First, we leverage the waist size dependence $S_\theta^{imp} \propto w_0^{-2}$ [Eq. (3)] to reduce imprecision for a fixed power P. Figure 3(b) shows a compilation of $P = 100$ μW measurements with different waist sizes by varying f. For $w_0 \leq 50$ μm, imprecision scales as w_0^{-2}, as expected. For $w_0 \gtrsim 60$ μm, it increases. We attribute this discrepancy to two sources of extra diffraction: (1) the finite ribbon width results in clipping, and (2) the ribbon imparts a position-dependent phase shift due to the photoelastic effect. Figure 2(d) shows a white light interferogram of the ribbon cross section, fit to a polynomial. The dominant fit parameter is quadratic, implying that the ribbon acts like a parabolic reflector with a radius of curvature $R_r \approx 3$ cm. The dashed curve in Fig. 3(b) is the Fraunhofer diffraction model accounting for both effects (see Supplement 1). The model fits the data well and implies that instead of decreasing monotonically with w_0, S_θ^{imp} is minimized for our device at $w_0 \approx 60$ μm.

In an effort to recover the ideal imprecision noise at large waist sizes, we investigated compensating for the phase profile of the ribbon. To this end, we adjusted the beam focus position z to engineer a finite radius of curvature, $R(z) = z(1 + (z_R/z)^2)$, at the ribbon surface, where $z_R = \pi w_0^2/\lambda$ is the Rayleigh length. As shown in Fig. 3(c), we recorded S_θ^{imp} while varying the focus position with $w_0 = 60$ μm and $P = 100$ μW, and found that the optimal position was indeed offset from the plane of the ribbon ($z = 0$). Overlaid is the same diffraction model as in Fig. 3(b), indicating that for $w_0 \leq 64$ μm, we can fully compensate for the phase of the ribbon [for $w_0 > 64$ μm, the maximum Gaussian wavefront curvature $R(z_R) = 2z_R$ is too small]. However, displacing the focus increases the spot size on the ribbon, thereby increasing the radiation pressure torque according to Eq. (4). In our case, the offset is $z/z_R \approx 1$, so backaction is a factor of $w^2/w_0^2 = 2$ times larger than the minimum.

After optimizing the beam waist and focus position, we turned our attention to increasing optical power. Figure 3(a) shows displacement spectra near mechanical resonance for several powers in the range $P = 0.01 - 10$ mW, calibrated to a thermal noise model (red line) [26]. In Fig. 3(d), we plot S_θ^{imp} versus P, averaged over two spectral regions shaded in Fig. 2(b): relatively close to (green points) and far from (blue points) resonance, respectively. Overlaid are models for the ideal imprecision and backaction of an optical lever [Eqs. (3) and (4)] and fits to a model including a constant extraneous noise floor. For $P < 1$ mW, we observe quantum noise scaling with an apparent total efficiency of $\eta = \eta_d \eta_{SD} \eta_\phi = 48\%$. With the detector placed in the far field ($L_{OL} \gg z_0 = .013$ m) corresponding to a quadrature angle of $\phi = -1.54$ rad, the measurement efficiency of the angular displacement quadrature is $\eta_\phi = 99\%$ [28], implying a detector efficiency of $\eta_d = 76\%$. At higher powers, off-resonant thermal noise of nearby mechanical modes limits S_θ^{imp} in the region close to resonance to 2.7×10^{-22} rad^2/Hz. In the region far

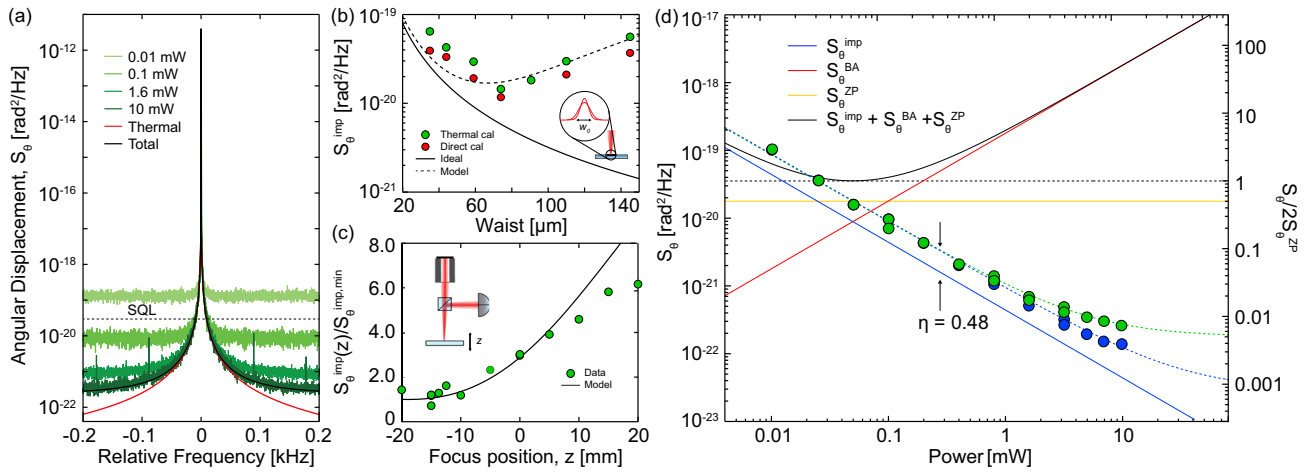

Fig. 3. (a) Optical lever measurement of the fundamental torsion mode for various probe powers P. Overlaid are models of thermal noise (red) and total noise for $P = 10$ mW (black). (b) Imprecision (noise floor) versus probe waist w_0 for $P = 100$ μW. Green and red points are calibrated by bootstrapping to the thermal model (green) and measuring the response of the SD to a lateral displacement (red) [26]. (c) Imprecision versus beam focus position z for $w_0 = 60$ μm, normalized to the inferred minimum at $z = -0.2$ cm. (d) Imprecision versus P for measurements as in (a). Blue and green points are averages over far-off-resonant (blue) and near-resonant (green) frequency bands in Fig. 2(c). Overlaid are models of imprecision (blue), backaction (red), zero-point motion (green), and their sum (black) for an ideal optical lever. Green and blue dashed lines are fits consistent with a measurement efficiency $\eta = 48\%$ and an extraneous imprecision 22 and 30 dB below the SQL, respectively.

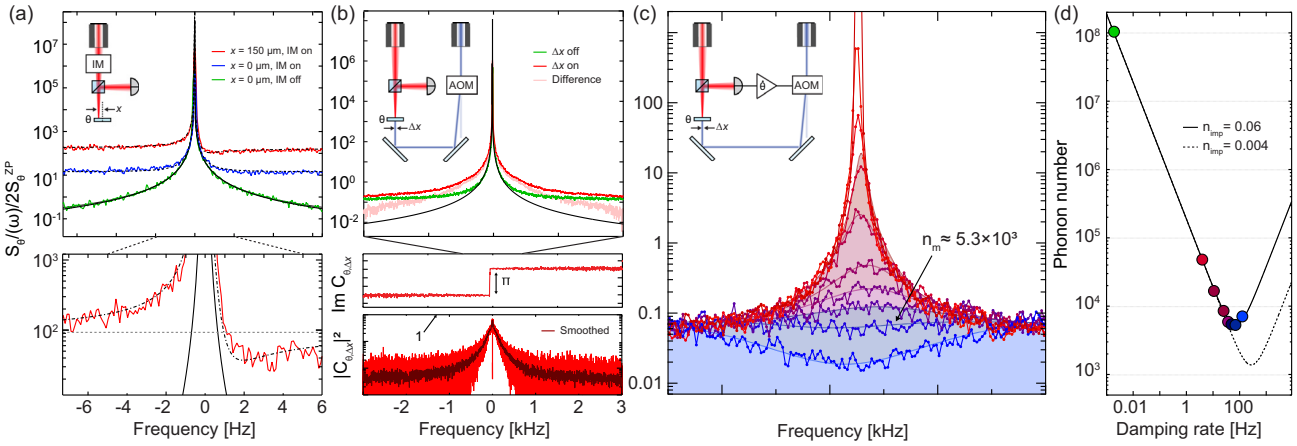

Fig. 4. Radiation pressure backaction and control of a torsion oscillator. (a) Classical backaction and imprecision–backaction correlations produced by an intensity-modulated (IM) OL beam misaligned from the torsion axis. (b) Simulation of radiation pressure torque shot noise by position modulating an auxiliary drive beam using an acousto-optic modulator (AOM). Above: thermal noise with (red) and without (green) auxiliary drive. Pink is the estimated backaction S_θ^{BA}. Below: coherence $C_{\theta\Delta x}$ between the OL measurement θ and drive beam displacement Δx (see main text). (c) Cold damping the torsion mode by imprinting the OL signal onto the drive beam position with a 90° phase shift near resonance. (d) Phonon number versus effective damping rate γ_{eff} by fitting the noise spectra in (c) to the closed loop model $n_{\mathrm{m}} = (\gamma_{\mathrm{eff}}/\gamma_{\mathrm{m}})(S_\theta(\omega_{\mathrm{m}}) + S_\theta^{\mathrm{imp}})/(2S_\theta^{\mathrm{ZP}})$ [30,32].

from resonance, we continue to observe quantum noise down to 1.4×10^{-22} rad^2/Hz at $P = 10$ mW. Scaling by $2S_\theta^{\mathrm{ZP}}$ on the right axis yields (independent of the absolute value of S_θ^{ZP} for a thermal noise calibration) a minimum effective noise quantum of $n_{\mathrm{imp}} = S_\theta^{\mathrm{imp}}/(2S_\theta^{\mathrm{ZP}}) = 0.004$, corresponding to an imprecision 18 dB below that at the SQL ($n_{\mathrm{imp}} = 1/4$) [30,31].

We now turn our attention to radiation pressure backaction in an OL measurement. To this end, as shown in Fig. 4, we carried out a series of experiments using the auxiliary position-modulated laser to simulate a stochastic and coherent (dynamical) backaction torque.

We first emphasize that the OL can be made immune to classical backaction due to laser intensity noise—modulation of the HG_{00} amplitude in Eq. (1)—when the probe beam is centered on the torsion axis. We explored this by comparing OL measurements with different lateral beam positions. As shown in Fig. 4(a), intensity noise was increased by probing with an external cavity diode laser (ECDL) current modulated with white noise. When the beam was centered on the ribbon, we observed negligible backaction but increased imprecision, as we were unable to fully balance out the added intensity noise on the SPD. When the beam was displaced, the total noise (physical motion and imprecision) increased and displayed an asymmetry about mechanical resonance. This asymmetry is a signature of imprecision–backaction correlations mediated by the mechanical susceptibility, $S_{\theta,\tau}[\omega] \propto \mathrm{Re}[\chi_{\mathrm{m}}]$, a classical analog to ponderomotive squeezing [33]. Fitting to a standard model [34] (dashed black line) implies that classical intensity noise backaction overwhelms thermal noise $S_\tau^{\mathrm{BA,IM}}[\omega] \approx 2.5 S_\theta^{\mathrm{th}}$ and can be suppressed by at least an order of magnitude.

Quantum torque backaction arises due to vacuum fluctuations of the HG_{10} mode in Eq. (1), physically manifesting as lateral beam fluctuations [24,29]. To simulate this form of "spatial" backaction [29], we applied white noise to the position-modulated drive beam until the motion it produced dominated the OL signal [Fig. 4(b)]. To confirm the backaction mechanism, we picked off a fraction of the drive beam and tracked its displacement Δx on an auxiliary SPD. We then computed the cross-spectrum $S_{\theta\Delta x}[\omega]$ with the OL signal θ. Figure 4(b) shows that the magnitude of the coherence $C_{\theta\Delta x} \equiv S_{\theta\Delta x}[\omega]/\sqrt{S_\theta[\omega]S_{\Delta x}[\omega]}$ approaches unity near the mechanical resonance, while the phase of the coherence (inset) exhibits a π phase shift. This behavior is consistent with mechanical motion dominated by radiation pressure torque noise [4,35].

Combining quantum-limited measurement and coherent backaction (feedback) enables ground-state preparation of a mechanical oscillator [30,36]. To explore this possibility, as a final demonstration, we imprinted the OL measurement onto the drive beam position with an appropriate phase shift to realize cold damping [37,38]. In the weak backaction limit, the phonon number of an oscillator cold-damped at rate γ_{eff} can be expressed as [30]

$$n_{\mathrm{m}} \approx \frac{\gamma_{\mathrm{m}}}{\gamma_{\mathrm{eff}}} n_{\mathrm{th}} + \frac{\gamma_{\mathrm{eff}}}{\gamma_{\mathrm{m}}} n_{\mathrm{imp}} \geq 2\sqrt{n_{\mathrm{th}} n_{\mathrm{imp}}}, \tag{6}$$

where $n_{\mathrm{th}} = S_\theta^{\mathrm{th}}/2S_\theta^{\mathrm{ZP}} = k_B T/\hbar\omega_{\mathrm{m}}$ is the thermal bath occupation [39]. Thus, combining our $n_{\mathrm{imp}} = 0.004$ OL measurement [Fig. 3(d)] and $n_{\mathrm{th}} = 1.2 \times 10^8$ torsion oscillator implies access to $n_{\mathrm{m}} \approx 1.4 \times 10^3$ from room temperature. Figures 4(c) and 4(d) show an experiment in which (for practical reasons related to the phase margin of our Red Pitaya controller [40]) we relax our imprecision to $n_{\mathrm{imp}} \approx 0.06$ and demonstrate cold damping to $n_{\mathrm{m}} \approx 5.3 \times 10^3$. Our data analysis procedure is described in Ref. [32].

In summary, we have explored the quantum limits of OL measurement by probing the high-Q torsion mode of a Si_3N_4 nanoribbon. A key aim is to highlight the potential for torsional quantum optomechanics experiments. Toward this end, we demonstrated a displacement imprecision 18 dB below that at the SQL, the working principle of radiation pressure shot noise in torque, and feedback cooling of a torsion oscillator from room temperature to 5.3×10^3 phonons. In conjunction with cryogenics, the natural immunity of the OL to technical noise augurs well for future cavity-free quantum optomechanics experiments. Indeed, at the time of this writing, we have become aware of a parallel study of Si_3N_4 nanoribbons with a "mirrored" OL capable

of imprecision at a level of $S_\theta^{\mathrm{imp}} \sim 10^{-12}\,\mathrm{rad}/\sqrt{\mathrm{Hz}}$ by rejecting classical beam pointing noise [41] [negligible in our current experiment (see Supplement 1)]. Applied to optimized nanoribbons with $Q \approx 10^8$ [26] and reduced effective curvature (see Supplement 1) suggests that $n_{\mathrm{m}} \sim 1$ may be accessible at cryogenic temperatures [specifically, for our device at 4 K with $Q = 10^8$ and $S_\theta^{\mathrm{imp}} \sim 10^{-12}\,\mathrm{rad}/\sqrt{\mathrm{Hz}}$, $n_{\mathrm{imp}} \sim 10^{-6}$ and $n_{\mathrm{th}} \sim 10^6$, in Eq. (6)]. Scaling nanoribbons to the centimeter scale [42] could also improve performance, owing to the favorable scaling law $n_{\mathrm{imp}} \propto h^3/(Q_0 w_{\mathrm{r}})$ [26] afforded by torsional dissipation dilution and optical leverage. Moreover, mass-loading Si_3N_4 nanoribbons have been shown not to diminish their torsional Q [26]. Thus, as emphasized by Shin *et al.* [41] and Cupertino *et al.* [43,44], torsional optomechanics may be a promising route to milligram-scale quantum gravity experiments and tests of the gravitational inverse square law [45]. Finally, we note that our work has interesting parallels to optomechanical torque magnetometry [46,47] and more recent efforts to optimally detect [48] and cool [49] libration modes of levitated dielectrics.

Note: As mentioned, we recently became aware of a related independent study by Shin *et al.* [41].

Funding. National Science Foundation (2239735, 2330310, 1725571); ARCS Foundation.

Acknowledgment. The authors thank Wenhua He, Morgan Choi, Jon Pratt, Stephan Schlamminger, and Jack Manley for helpful discussions. We also thank Atkin Hyatt and Mitul Dey Chowdhury for the photograph in Fig. 1. CMP acknowledges support from the ARCS Foundation. ARA acknowledges support from a CNRS-UArizona iGlobes fellowship. The reactive ion etcher used for this study was funded by an NSF MRI.

Disclosures. The authors declare no conflicts of interest.

Data availability. Data underlying the results presented in this paper are not publicly available at this time but may be obtained from the authors upon reasonable request.

Supplemental document. See Supplement 1 for supporting content.

REFERENCES AND NOTES

1. E. F. Nichols and G. F. Hull, "The pressure due to radiation," in *Proceedings of the American Academy of Arts and Sciences* (JSTOR, 1903), Vol. **38**, pp. 559–599.
2. B. P. Abbott, R. Abbott, T. Abbott, *et al.*, "Observation of gravitational waves from a binary black hole merger," Phys. Rev. Lett. **116**, 061102 (2016).
3. C. A. Coulomb, "Premier mémoire sur l'électricité et le magnétisme," Hist. R. Acad. Sci., 569–577 (1785).
4. T. P. Purdy, R. W. Peterson, and C. Regal, "Observation of radiation pressure shot noise on a macroscopic object," Science **339**, 801–804 (2013).
5. J. Aasi, J. Abadie, B. Abbott, *et al.*, "Enhanced sensitivity of the LIGO gravitational wave detector by using squeezed states of light," Nat. Photonics **7**, 613–619 (2013).
6. I. Shomroni, L. Qiu, D. Malz, *et al.*, "Optical backaction-evading measurement of a mechanical oscillator," Nat. Commun. **10**, 2086 (2019).
7. D. Ganapathy, W. Jia, M. Nakano, *et al.*, "Broadband quantum enhancement of the LIGO detectors with frequency-dependent squeezing," Phys. Rev. X **13**, 041021 (2023).
8. D. Mason, J. Chen, M. Rossi, *et al.*, "Continuous force and displacement measurement below the standard quantum limit," Nat. Phys. **15**, 745–749 (2019).
9. W. Jia, V. Xu, K. Kuns, *et al.*, "LIGO operates with quantum noise below the Standard Quantum Limit," arXiv (2024).
10. D. Carney, G. Krnjaic, D. C. Moore, *et al.*, "Mechanical quantum sensing in the search for dark matter," Quantum Sci. Technol. **6**, 024002 (2021).
11. M. Rademacher, J. Millen, and Y. L. Li, "Quantum sensing with nanoparticles for gravimetry: when bigger is better," Adv. Opt. Technol. **9**, 227–239 (2020).
12. R. Jones, "Some developments and applications of the optical lever," J. Sci. Instrum. **38**, 37 (1961).
13. E. G. Adelberger, J. Gundlach, B. Heckel, *et al.*, "Torsion balance experiments: a low-energy frontier of particle physics," Prog. Part. Nucl. Phys. **62**, 102–134 (2009).
14. T. Westphal, H. Hepach, J. Pfaff, *et al.*, "Measurement of gravitational coupling between millimetre-sized masses," Nature **591**, 225–228 (2021).
15. S. Alexander, L. Hellemans, O. Marti, *et al.*, "An atomic-resolution atomic-force microscope implemented using an optical lever," J. Appl. Phys. **65**, 164–167 (1989).
16. C. A. Putman, B. G. De Grooth, N. F. Van Hulst, *et al.*, "A detailed analysis of the optical beam deflection technique for use in atomic force microscopy," J. Appl. Phys. **72**, 6–12 (1992).
17. C. A. Putman, B. G. De Grooth, N. F. Van Hulst, *et al.*, "A theoretical comparison between interferometric and optical beam deflection technique for the measurement of cantilever displacement in AFM," Ultramicroscopy **42**, 1509–1513 (1992).
18. S. M. Barnett, C. Fabre, and A. Maître, "Ultimate quantum limits for resolution of beam displacements," Eur. Phys. J. D **22**, 513–519 (2003).
19. V. Delaubert, N. Treps, C. C. Harb, *et al.*, "Quantum measurements of spatial conjugate variables: displacement and tilt of a Gaussian beam," Opt. Lett. **31**, 1537–1539 (2006).
20. M. T. Hsu, V. Delaubert, P. K. Lam, *et al.*, "Optimal optical measurement of small displacements," J. Opt. B **6**, 495 (2004).
21. W. He, C. N. Gagatsos, D. J. Wilson, *et al.*, "Optimum classical beam position sensing," arXiv (2024).
22. N. Treps, N. Grosse, W. P. Bowen, *et al.*, "A quantum laser pointer," Science **301**, 940–943 (2003).
23. R. C. Pooser and B. Lawrie, "Ultrasensitive measurement of microcantilever displacement below the shot-noise limit," Optica **2**, 393–399 (2015).
24. S. Hao and T. P. Purdy, "Back action evasion in optical lever detection," Optica **11**, 10–17 (2024).
25. A. A. Clerk, M. H. Devoret, S. M. Girvin, *et al.*, "Introduction to quantum noise, measurement, and amplification," Rev. Mod. Phys. **82**, 1155–1208 (2010).
26. J. R. Pratt, A. R. Agrawal, C. A. Condos, *et al.*, "Nanoscale torsional dissipation dilution for quantum experiments and precision measurement," Phys. Rev. X **13**, 011018 (2023).
27. E. Fradgley, C. French, L. Rushton, *et al.*, "Quantum limits of position-sensitive photodiodes," Opt. Express **30**, 39374–39381 (2022).
28. Y. Enomoto, K. Nagano, and S. Kawamura, "Standard quantum limit of angular motion of a suspended mirror and homodyne detection of a ponderomotively squeezed vacuum field," Phys. Rev. A **94**, 012115 (2016).
29. C. M. Pluchar, W. He, J. Manley, *et al.*, "Imaging-based quantum optomechanics," arXiv (2024).
30. D. J. Wilson, V. Sudhir, N. Piro, *et al.*, "Measurement-based control of a mechanical oscillator at its thermal decoherence rate," Nature **524**, 325–329 (2015).
31. J. D. Teufel, T. Donner, M. Castellanos-Beltran, *et al.*, "Nanomechanical motion measured with an imprecision below that at the standard quantum limit," Nat. Nanotechnol. **4**, 820–823 (2009).
32. C. M. Pluchar, A. R. Agrawal, E. Schenk, *et al.*, "Towards cavity-free ground-state cooling of an acoustic-frequency silicon nitride membrane," Appl. Opt. **59**, G107–G111 (2020).
33. F. Marino, F. S. Cataliotti, A. Farsi, *et al.*, "Classical signature of ponderomotive squeezing in a suspended mirror resonator," Phys. Rev. Lett. **104**, 073601 (2010).
34. V. Sudhir, R. Schilling, S. A. Fedorov, *et al.*, "Quantum correlations of light from a room-temperature mechanical oscillator," Phys. Rev. X **7**, 031055 (2017).
35. C. M. Pluchar, A. R. Agrawal, and D. J. Wilson, "Thermal intermodulation backaction in a high-cooperativity optomechanical system," Optica **10**, 1543–1550 (2023).
36. M. Rossi, D. Mason, J. Chen, *et al.*, "Measurement-based quantum control of mechanical motion," Nature **563**, 53–58 (2018).
37. M. Poggio, C. Degen, H. Mamin, *et al.*, "Feedback cooling of a cantilever's fundamental mode below 5 mK," Phys. Rev. Lett. **99**, 017201 (2007).

38. J.-M. Courty, A. Heidmann, and M. Pinard, "Quantum limits of cold damping with optomechanical coupling," Eur. Phys. J. D **17**, 399–408 (2001).
39. A more precise bound for n_{m}—ignoring the finite Qf of the oscillator, which limits $n_{\mathrm{m}} \gtrsim (k_B T/h)/(Qf) \sim 1$ in our case—is $n_{\mathrm{m}} + 0.5 \geq 2\sqrt{(n_{\mathrm{th}} + n_{\mathrm{BA}})n_{\mathrm{imp}}} = \sqrt{(1 + C_{\mathrm{q}}^{-1})/(2\eta)}$, where $n_{\mathrm{BA}} = S_\theta^{\mathrm{BA}}/(2S_\theta^{\mathrm{ZP}})$ is the phonon-equivalent quantum backaction, $C_q = n_{\mathrm{BA}}/n_{\mathrm{th}}$ is the quantum cooperativity, and η is the measurement quantum efficiency [30,36]. In our experiment $\eta \sim 1$ and $C_q \sim 10^{-6}$, such that Eq. (6) is a good approximation.
40. L. Neuhaus, M. Croquette, R. Metzdorff, *et al.*, "FPGA-based feedback control of quantum optics experiments with the open source software package PyRPL," arXiv (2023).
41. D. C. Shin, T. M. Hayward, D. Fife, *et al.*, "Laser cooling a centimeter-scale torsion pendulum," arXiv (2024).
42. A. Cupertino, D. Shin, L. Guo, *et al.*, "Centimeter-scale nanomechanical resonators with low dissipation," Nat. Commun. **15**, 4255 (2024).
43. S. Agafonova, P. Rossello, M. Mekonnen, *et al.*, "Laser cooling a 1-milligram torsional pendulum to 240 microkelvins," arXiv (2024).
44. K. Komori, Y. Enomoto, C. P. Ooi, *et al.*, "Attonewton-meter torque sensing with a macroscopic optomechanical torsion pendulum," Phys. Rev. A **101**, 011802 (2020).
45. J. Manley, C. Condos, S. Schlamminger, *et al.*, "Microscale torsion resonators for short-range gravity experiments," arXiv (2024).
46. P. Kim, B. Hauer, C. Doolin, *et al.*, "Approaching the standard quantum limit of mechanical torque sensing," Nat. Commun. **7**, 13165 (2016).
47. M. Wu, N. L.-Y. Wu, T. Firdous, *et al.*, "Nanocavity optomechanical torque magnetometry and radiofrequency susceptometry," Nat. Nanotechnol. **12**, 127–131 (2017).
48. F. Tebbenjohanns, A. Militaru, A. Norrman, *et al.*, "Optimal orientation detection of an anisotropic dipolar scatterer," Phys. Rev. A **105**, 053504 (2022).
49. J. Gao, F. van der Laan, J. A. Zielińska, *et al.*, "Feedback cooling a levitated nanoparticle's libration to below 100 phonons," Phys. Rev. Res. **6**, 033009 (2024).